Sun, J Material Sci Eng 2018, 7:2
DOI: 10.4172/2169-0022.1000436

Journal of Material Sciences & Engineering

Research Article Open Access

Growth of Columnar Co_3Pt Strucrure with Ru Buffer Layer at Room Temperature

An-Cheng Sun*

Department of Chemical Engineering and Materials Science, Yuan Ze University, Chung-Li, 32003, Taiwan

Abstract

Magnetic Co_3Pt films were sputtered on a Ru(0002)/Pt(111) bilayer on glass substrate at room temperature. The effects of a Ru buffer layer thickness (*t* nm) on magnetic properties and microstructures were studied. AFM surface roughness results revealed that the root mean square roughness (R_{rms}) of the Ru/Pt bilayer surface is smaller than 1.5 nm. Granular Ru topography was observed as *t* is larger than 7 nm, which played an important role in influencing the magnetic properties and microstructures of Co_3Pt thin film. In this study, Ru(0002) grew along the Pt(111) underlayer and then became a template for epitaxially growing Co_3Pt(0002) film, in order to enhance the perpendicular magnetic anisotropy (PMA). Maximum H_c were obtained as *t*=15, due to the columnar structure formed in the whole Co_3Pt/Ru/Pt film. It demonstrates that a Ru buffer layer is helpful to enhance the PMA of Co_3Pt magnetic thin film and increase out-of-plane squareness ($S_\perp$) and H_c.

Keywords: Perpendicular magnetic anisotropy; Co_3Pt thin film; Buffer layer thickness; Epitaxial growth

Introduction

In order to achieve a higher areal density of magnetic recording media, new developments are constantly coming out one after another. Recently, magnetic tunneling junction (MTJ) based spin transfer torque magneto resistive random access memory (STT-MRAM) has been regarded as the next generation temporary data storage device [1-3]. In this case, material with large magnetocrystalline anisotropy (K_u), high coercivity (H_c) and good chemical stability is necessary for the fix layer in an MTJ cell. Furthermore, material for a fix layer with a high perpendicular magnetic anisotropy (PMA) can make cells become perpendicular MTJ (p-MTJ), which can further increase recording density [3]. Thus, high PMA $L1_0$-type FePt and CoPt magnetic alloy thin film has attracted a great deal of research in recent years [4-10]. However, an $L1_0$ phase transformation temperature is too high, becoming a drawback for further application. Recently, Co_3Pt with an HCP structure has been regarded as a promising candidate to replace $L1_0$-type FePt and CoPt due to its lower formation temperature (RT~350°C) and similar magnetic properties such as large K_u (~2×10^7 erg/cm^3) and PMA ($S_\perp$~0.9), compared with $L1_0$-type FePt and CoPt [11-16]. Additionally, lower Pt content can make this structure more economical. In order to develop an HCP structural Co_3Pt with high PMA, costly single crystal substrates such as MgO(111) and Al_2O_3(0001) were adopted [17-20], suggesting an obvious limitation in future applications. Thus, it is necessary to fabricate HCP structural Co_3Pt on glass substrate and still retain its attractive magnetic properties. But HCP structural Co_3Pt difficultly grows on glass substrate due to the amorphous substrate plane.

Usually, textured underlayer was adopted to enhance the PMA of magnetic layer on glass substrate [15,16,21], because small lattice mismatch (δ) between magnetic layer and underlayer helps PMA phase epitaxially grows on the lattice sites of underlayer and consequently induced higher PMA of magnetic layer. The δ is used to illustrate the extent of lattice differences of two different materials during epitaxial growth. The δ between two different materials, α and β, can be calculated by the following formula [22]:

$$\delta = \frac{a_\alpha - a_\beta}{a_\alpha} \tag{1}$$

where a_α and a_β are the lattice parameters of materials α and β, respectively.

Pt(111) shows a flat surface and similar lattice parameters to a Co_3Pt(0002) plane. Thus, the lattice mismatch (δ=7.9%) at Pt(111)/Co_3Pt(0002) interface provides a template for epitaxially growing Co_3Pt with (0002) orientation [23]. However, if the δ could be further reduced, Co_3Pt films with more (0002) orientation would be expected. To achieve that, HCP Ru(0002) is a proper choice. Figure 1 depicts δ between Co_3Pt(0002), Ru(0002), and Pt(111). Lattice parameters of Co_3Pt(0002) $[11\bar{2}0]$, Ru(0002)$[11\bar{2}0]$, and Pt(111) [110] are 0.255, 0.270 and 0.277 nm, respectively. Therefore, δ between Ru(0002) $[11\bar{2}0]$ and Co_3Pt(0002) $[11\bar{2}0]$ is 5.9%, which is smaller than the lattice misfit between Co_3Pt(0002)$[11\bar{2}0]$ and Pt(111)[110]. However, it is difficult to deposit pure HCP Ru(0002) structural film directly on glass substrate in our experience; usually, the second phase appears easily. But using a Pt(111) to induce the Ru(0002) is workable since the δ between Pt(111) and Ru(0002) is 2.6%, which is helpful for Ru(0002) growth. Therefore, an HCP Co_3Pt(0002) structure is expected to be fabricated by adopting a Pt/Ru bilayer film. In this study, Ru layers with

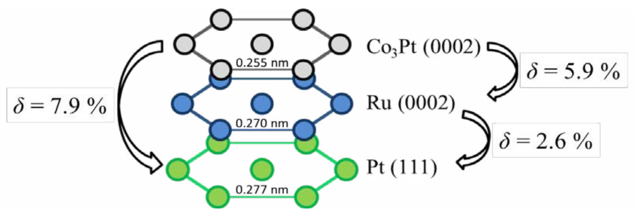

Figure 1: Lattice mismatch (δ) between Pt(111), Ru(0002), and Co_3Pt(0002).

***Corresponding author:** An-Cheng Sun, Professor, Department of Chemical Engineering and Materials Science, Yuan Ze University, Chung-Li, 32003, Taiwan, Tel: 886-3-4638800, Extn. 2554; Fax: 886-3-4559373; E-mail: acsun@saturn.yzu.edu.tw

Received February 27, 2018; **Accepted** March 13, 2018; **Published** March 23, 2018

Citation: Sun AC (2018) Growth of Columnar Co_3Pt Strucrure with Ru Buffer Layer at Room Temperature. J Material Sci Eng 7: 436. doi: 10.4172/2169-0022.1000436

different thicknesses (t nm) were prepared as the buffer layer between a Pt underlayer and a Co_3Pt magnetic layer, and the effect of Ru buffer layer thickness on magnetic properties and microstructures of Co_3Pt films was investigated.

Experimental Section

In this study, HCP structural Co_3Pt(10 nm)/Ru(t nm)/Pt(20 nm)/glass substrate was fabricated by a sputtering method in a high vacuum magnetron sputtering system. The base pressure of the chamber was greater than 2×10^{-7} Torr. Argon was selected to be the working gas and the pressure was set to 10 mTorr. Direct current (DC) power was adopted to supply the sputtering system. Before sputtering the magnetic Co_3Pt layer, Ru layer with varied t was sputtered on a 20 *nm*-thick textured Pt(111) underlayer on glass substrate at 350°C, where t was 0, 7, 15 and 25 nm, respectively. After that, the substrate was cooled to room temperature (RT) for depositing Co_3Pt film at a 10 nm thickness. Two-inch Co, Pt, and Ru targets with purity levels higher than 99.99 at.% was adopted as the sputtering sources. The Pt content in the Co-Pt alloy thin film was controlled by adjusting the number of Pt chips on the Co target. The chemical composition of Co-Pt film was 76 at.% Co and 24 at.% Pt, which was confirmed by energy dispersion spectroscopy (EDS) equipped on a field-emission scanning electron microscope (FE-SEM). The thickness and surface roughness of the films were checked by an atomic force microscope (AFM). The surface morphology was observed by SEM. Magnetic properties were measured by a vibrating sample magnetometer (VSM). The crystallization was characterized by X-Ray diffractometer (XRD) with Cu-$K\alpha$ radiation. The microstructure was investigated using a high-resolution transmission electron microscope (HR-TEM) with 200 keV accelerating voltages.

Results and Discussion

In order to understand the effect of the Ru thickness on surface roughness in Ru/Pt bilayers, the topography of Ru(t nm)/Pt(20 nm) bilayers were identified by AFM and shown in Figure 2a-2d. Figure 2e is the relationship between t and the root mean square roughness (R_{rms}) of Ru/Pt bilayers. All the bilayer films have flat surface, where the R_{rms} of surfaces are less than 1.5 nm. In Figure 2a, numerous small dots are observed at t=0, which shows the lowest R_{rms} (0.23 nm) in Ru/Pt bilayers. Further increasing t would increase the R_{rms}. When t=7, small particles could be observed on the surface (marked by white arrow in Figure 2b), so called granular topography. The amount of particles increase as t is increased to 15 nm (Figure 2c). The particles size was also raised and the maximum R_{rms} (R_{rms}=1.36) was obtained. When t keeps increasing to 25 nm (Figure 2d), the amount and size of particles decreased slightly, leading the R_{rms} decreasing to 0.53 nm. Apparently, the particles played an important role in affecting the R_{rms} in Ru/Pt bilayer. Next, Co_3Pt magnetic layer was sputtered on the Ru/Pt bilayer, therefore it is expected that granular topography influence Co_3Pt film growth.

Figure 3a-3d show hysteresis loops of Co_3Pt(10 nm)/Ru(t nm)/Pt(20 nm) films, where t=(a) 0, (b) 7, (c) 15 and (d) 25 nm. Figure 3f exhibits the functions of out-of-plane squareness ($S_\perp$) and coercivity ($H_{c\perp}$) on the thickness of Ru layer. Without a Ru buffer layer (t=0), the film shows lower $H_{c\perp}$ (~0.23 kOe) and $S_\perp$ (~0.23). Then, the $H_{c\perp}$ and $S_\perp$ increase as t increases. The maximum $H_{c\perp}$ (~1.7 kOe) and $S_\perp$(~0.43) appear at t=15, indicating that a higher amount of perpendicular hard magnetic structure exists in the Co_3Pt film. Further increasing t decreased $H_{c\perp}$ and $S_\perp$. Combining with R_{rms} in Ru/Pt bilayer, as shown in Figure 2, can obtain that the highest $H_{c\perp}$ with the highest R_{rms} (1.36 nm) is at t=15. Increasing t to 25 nm leads R_{rms} to decline and further reduce $H_{c\perp}$ and $S_\perp$.

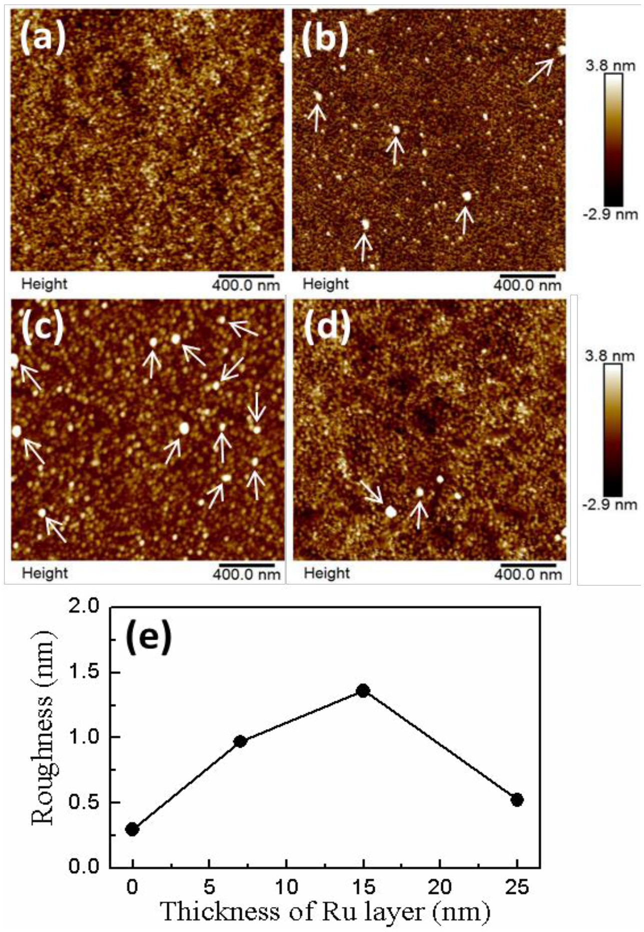

Figure 2: Surface topography of Ru(t nm)/Pt(20 nm) bilayers, where t=(a) 0, (b) 7, (c) 15, and (d) 25 nm. (e) is the relationship between t and R_{rms}.

Figure 4a shows XRD patterns of Co_3Pt(10 nm)/Ru(t nm)/Pt(20 nm), where t=0, 7, 15 and 25 nm, respectively. It is clear to see the strong Pt(111) diffraction peaks in all samples, indicating formation of a textured Pt(111) underlayer. However, Co_3Pt(0002) diffraction peaks are weak at t=0, revealing poor crystallization. Increasing the t to 7 nm quickly enhances the intensity of the Ru(0002) peak. Although little $A1$ CoPt(111) forms at 2θ=41.9°, a clear Co_3Pt(0002) diffraction peak appears at 2θ=43.2°, indicating the Ru(0002) has the benefit to grow a Co_3Pt(0002) phase. However, more Co_3Pt(0002) does not increase the $H_{c\perp}$. Further increasing the t to 25 nm presents highest Ru(0002) peak, but lower Co_3Pt(0002) peak. Figure 4b presents the lattice constants of FCC Pt(111), HCP Ru(0002), and HCP Co_3Pt(0002), calculating from Figure 4a. The dash lines are the lattice constants form bulk material [24-26]. All the Pt(111) show a similar lattice constant, indicating that the underlayer provides a stable template for Ru film growth. When t > 7, the lattice spacing of Ru(0002) increases with t. As lattice constant of Pt is larger than Ru, this phenomena suggests that the Ru(0002) lattice is adjusted by the Pt(111) plane. Increasing the thickness of Ru layer continuously expands its lattice constant. The upper Co_3Pt(0002) layer is also fitted with a lattice spacing with Ru(0002) when t>7, evidencing the epitaxial growth between Ru(0002) and Co_3Pt(0002) planes [21,27].

Citation: Sun AC (2018) Growth of Columnar Co_3Pt Strucrure with Ru Buffer Layer at Room Temperature. J Material Sci Eng 7: 436. doi: 10.4172/2169-0022.1000436

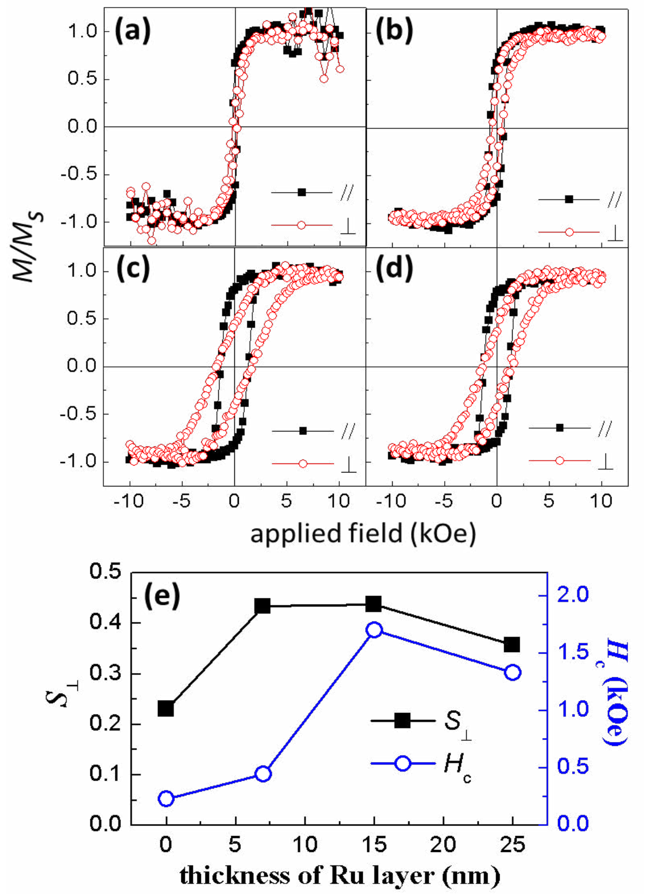

Figure 3: Hysteresis loops of Co_3Pt(10 nm)/Ru(t nm)/Pt(20 nm), where t=(a) 0, (b) 7, (c) 15, and (d) 25 nm. (e) is the relationship between $S_\perp$, H_c and t.

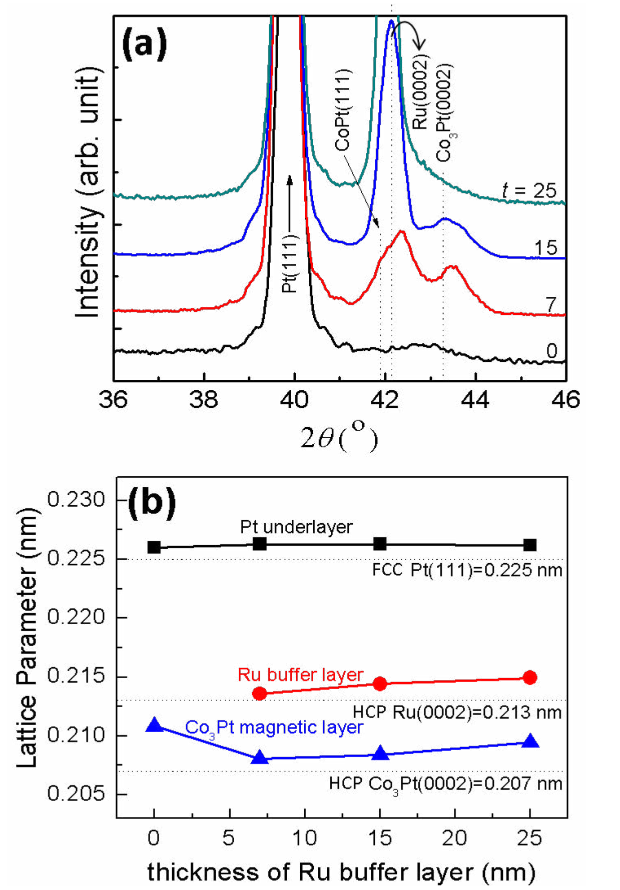

Figure 4: (a) XRD patterns of Co_3Pt(10 nm)/Ru(t nm)/Pt(20 nm), where t=0, 7, 15 and 25. (b) is corresponding calculated lattice spacing for Pt(111), Ru(0002), and Co_3Pt(0002).

A comparison of Figures 2e, 3e and 4b finds that the surface roughness between Ru(0002) and Co_3Pt(0002) is the major effect on crystal quality of Co_3Pt(0002) structure. Thus, losing granular topography at t=25 decreases the amount of Co_3Pt(0002) orientation, thereby achieving a low $S_\perp$.

In order to understand the granular topography effect, the internal microstructures of Co_3Pt(10 nm)/Ru(t nm)/Pt(20 nm) films are shown in Figure 5. Figure 5a-5c show cross-sectional TEM bright field images of Co_3Pt(10 nm)/Ru(t nm)/Pt(20 nm) trilayer films with t=0, 7 and 15 nm, and the corresponding magnified images are shown in Figures 5d-5f, respectively. In Figure 5a, a flat interface between Pt and Co_3Pt can be clearly observed at t=0, which is in agreement with the AFM results (Figure 2a). In the enlarged image (Figure 5d), Pt(111) lattice images appeared. However, a Co_3Pt lattice image seems unclear observation, evidencing that the flat Pt(111) underlayer is insufficient to grow HCP Co_3Pt(0002) at RT. This result is also predicted by the XRD, which show a strong Pt(111) but a weak Co_3Pt(0002) diffraction peak. When t increases to 7 nm, as shown in Figure 5b, the film shows continuous film structure with less grain boundary, which has a less pinning site for the magnetic reversal process and further reduces H_c [28,29]. Figure 5e shows the corresponding magnified image. Very clear lattice images are observed and the lattice distances are identified as 0.224 nm, 0.215 nm and 0.208 nm, which correlate with Pt(111), Ru(0002), and Co_3Pt(0002), respectively. This is the proof that a Ru(0002) buffer layer grows along the Pt(111) underlayer and further induces the formation

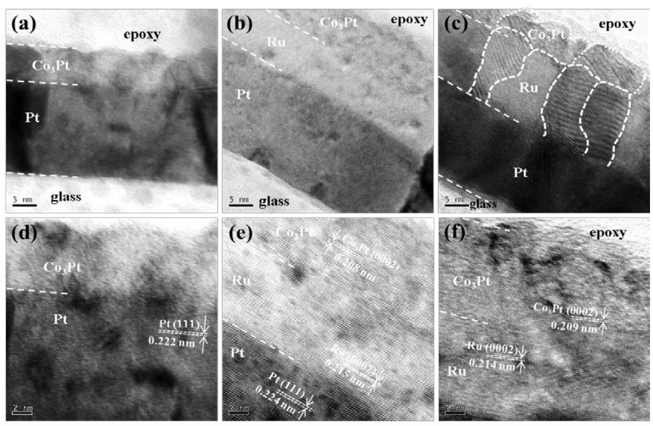

Figure 5: Cross-sectional TEM images of Co_3Pt(10 nm)/Ru(t nm)/Pt(20 nm), where t=(a) 0, (b) 7, and (c) 15 nm. The corresponding magnified images are shown in (d)–(f), respectively.

of Co_3Pt(0002). With a further increase of t to 15 nm, as shown in Figure 5c, it is clear that the Ru buffer layer transfers into a columnar structure (marked as white dash line), which resulting granular topography in the AFM results (Figure 2d). This columnar growth behavior may result in a higher R_{rms}. Granular structural buffer layers provide a template which helps Co_3Pt to grow along it and allows Co_3Pt to become a columnar structure which makes the film discontinuous and obtains higher $H_{c\perp}$. In Figure 5f, the clear Ru lattice is helpful for $Co_3Pt(0002)$ growth at RT.

Conclusion

In this study, the correlation between magnetic properties and microstructures of Co_3Pt films sputtered on various thicknesses of Ru buffer layer at RT were investigated. Results point out that the Ru/Pt bilayer shows a granular topography. When t=7, the Co_3Pt film shows a high $S_{\perp}$ but a lower $H_{c\perp}$ due to less pinning site in the continuous magnetic film structure. The maximum R_{rms} can be observed at t=15, which also shows the greatest $H_{c\perp}$. The microstructure indicates that a Ru(0002)/Pt(111) bilayer structure could enhance the $Co_3Pt(0002)$ phase and $S_{\perp}$. The films form a columnar structure and further increase $H_{c\perp}$ to 1.7 kOe when t=15. Kept increasing t to 25 nm decreases $H_{c\perp}$ and $S_{\perp}$. Our results indicate that a Ru buffer layer is helpful for $Co_3Pt(0002)$ growth of RT-deposited Co_3Pt magnetic thin films, which can be the basis for future development of Co_3Pt magnetic films at RT.

References

1. Tudu B, Tiwari A (2017) Recent developments in perpendicular magnetic anisotropy thin films for data storage applications. Vacuum 146: 329-341.
2. Kan JJ, Gottwald M, Park C, Zhu X, Kang SH (2015) Thermally robust perpendicular STT-MRAM free layer films through capping layer engineering. IEEE Transactions on Magnetics 51: 1-5.
3. Ikeda S, Miura K, Yamamoto H, Mizunuma K, Gan HD, et al. (2010) A perpendicular-anisotropy CoFeB–MgO magnetic tunnel junction. Nature Materials 9: 721-724.
4. Liu L, Zhang L, Liang L, Ohsasa K, Koyama T, et al. (2016) Microstructure of L10 FePt thin films with anisotropic interfacial energy coefficients and anisotropic atomic mobilities. Journal of Alloys and Compounds 682: 176-179.
5. Ohtake M, Itabashi A, Futamoto M, Kirino F, Inaba N, et al. (2014) Control of c-Axis Orientation of $L1_0$ Ordered FePt, CoPt, and FePd Alloy Thin Films Deposited on MgO(001) Substrates, IEEE Trans Magn, 50.
6. Ho H, Zhu J, Kulovits A, Laughlin DE, Zhu JG (2014) Quantitative transmission electron microscopy analysis of multi-variant grains in present L10-FePt based heat assisted magnetic recording media. Journal of Applied Physics 116: 193510.
7. Ohtake M, Itabashi A, Kirino F, Futamoto M (2013) $L1_0$ Ordered FePd, FePt, and CoPt Thin Films With Flat Surfaces Prepared on MgO (110) Single-Crystal Substrates. IEEE Transactions on Magnetics 49: 3295-3298.
8. Wang J, Hata S, Takahashi YK, Sepehri-Amin H, Varaprasad BCS, et al. (2015) Effect of MgO underlayer misorientation on the texture and magnetic property of FePt–C granular film. Acta Materialia 91: 41-49.
9. Zhao ZL, Ding J, Yi JB, Liu BH, Chen JS, et al. (2005) Nanostructured FePt thin films with high coercivity. J Mater Sci and Technol 21: 43-46.
10. Wang LW, Shih WC, Wu YC, Lai CH (2012) Promotion of [001]-oriented L10-FePt by rapid thermal annealing with light absorption layer. Applied Physics Letters 101: 252403.
11. Park KW, Oh YW, Kim DH, Kim JY, Park BG (2016) Effect of sputtering pressure on stacking fault density and perpendicular magnetic anisotropy of CoPt alloys. Journal of Physics D: Applied Physics 49: 345002.
12. Hara R, Hayakawa K, Ebata K, Sugita R (2016) Effect of aging and annealing on perpendicular magnetic anisotropy of ultra-thin CoPt films. AIP Advances 6: 056117.
13. Tham KK, Hinata S, Saito S (2015) Effect of Topological Bumpy Surface Underlayer on Compositionally Modulated Atomic Layer Stacking in High K_u hcp Co_{80} Pt_{20} Film With (00.2) Crystallographic Texture Orientation. IEEE Transactions on Magnetics 51: 1-4.
14. Chen YS, Dai HY, Hsu YW, Ou SL, Chen SW, et al. (2017) Room temperature deposition of perpendicular magnetic anisotropic Co3Pt thin films on glass substrate. Journal of Magnetism and Magnetic Materials 425: 57-62.
15. Mifuji S, Sakuma H, Ishii K (2005) Co–Pt/Pt thin films with perpendicular magnetization and a high coercivity prepared by gas flow sputtering. Journal of Applied Physics 97: 10N102.
16. Yuan FT, Sun AC, Hsu JH (2010) Effect of underlayer (Pt, Ru, Au, Ag) on L11 ordering in sputtered CoPt thin films. Scripta Materialia 62: 762-765.
17. Yamada Y, Van Drent WP, Abarra EN, Suzuki T (1998) High perpendicular anisotropy and magneto-optical activities in ordered Co 3 Pt alloy films. Journal of Applied Physics, 83: 6527-6529.
18. Harp GR, Weller D, Rabedeau TA, Farrow RFC, Toney MF (1993) Magneto-optical Kerr spectroscopy of a new chemically ordered alloy: Co 3 Pt. Physical Review Letters 71: 2493.
19. Moraitis G, Parlebas JC, Khan MA (1996) The band structure of chemically ordered. Journal of Physics: Condensed Matter 8: 1151-1161.
20. Sato H, Shimatsu T, Okazaki Y, Muraoka H, Aoi H, et al. (2008) Fabrication of L 1 1 type Co-Pt ordered alloy films by sputter deposition. Journal of Applied Physics 103: 07E114.
21. Pandey KKM, Chen JS, Chow GM, Lim BC (2009) Seedlayer interface enhanced magnetic anisotropy in CoPt (0 0 0 2)-textured films. Journal of Magnetism and Magnetic Materials 321: 3236-3240.
22. Xu Y, Chen JS, Dai D, Wang JP (2002) FePt fct-[001] texture prepared at lower temperature for high areal density perpendicular recording. IEEE Transactions on Magnetics 38: 2042-2044.
23. Porter DA, Easterling KE, Sherif M (2009) Crystal Interfaces and Microstructure, in Phase transformations in Metals and Alloys, pp: 152-155.
24. Joint committee on powder diffraction standards (JCPDS) (1997) card No. 870646
25. Joint committee on powder diffraction standards (JCPDS) (2002) card No. 89-4903
26. Hinata S, Yamane A, Saito S (2016) Effect of additional elements on compositional modulated atomic layered structure of hexagonal Co80Pt20 alloy films with superlattice diffraction. AIP Advances 6: 056124.
27. Xu Y, Chen JS, Wang JP (2002) In situ ordering of FePt thin films with face-centered-tetragonal (001) texture on Cr 100−x Ru x underlayer at low substrate temperature. Applied Physics Letters 80: 3325-3327.
28. Trichy GR, Chakraborti D, Narayan J, Prater JT (2007) Epitaxial FePt thin films and nanodots integrated with Si (100). Journal of Physics D: Applied Physics 40: 7273-7280.
29. Giannopoulos G, Speliotis T, Niarchos D (2014) Study of microstructure and magnetic properties of L10 FePt/SiO2 thin films. EPJ Web of Conferences 75: 06014.